

Breakup Effect on the Reactions of ${}^4,{}^6\text{He}$ and ${}^6\text{Li}$

Badawy ABU-IBRAHIM

*Department of Physics, Niigata University, Niigata 950-2181, Japan
and*

Department of Physics, Cairo University, Giza 12613, Egypt

(Received September 1, 2004)

The breakup effect on the scattering and reaction of ${}^4,{}^6\text{He}+p$, ${}^{12}\text{C}$, ${}^{40}\text{Ca}$ and ${}^6\text{Li}+p$ at energies of 50–800 MeV/nucleon has been studied in the framework of the eikonal approximation. The eikonal phase-shift functions have been calculated completely employing Monte Carlo integration. Realistic 6-nucleon wave functions for the ${}^6\text{He}$ and ${}^6\text{Li}$ nuclei have been used. The dynamic polarization potentials have been determined. We find that the breakup effect is minimal at an incident energy of 200 MeV/nucleon. At this energy, the imaginary part of the polarization potential changes sign (negative to positive with increasing energy). The real part of the polarization potential also changes sign (repulsive to attractive) around 400 MeV/nucleon. This sign change depends neither on the target nor the projectile. It depends only on the ratio of the real to the imaginary parts of the underlying nucleon-nucleon (or nucleon-target) potential. The breakup effect is stronger in ${}^6\text{He}$ than in ${}^6\text{Li}$.

§1. Introduction

Halo nuclei are a special case of radioactive beams for which the last nucleons are very weakly bound, with separation energies of the order of 0.5 MeV or less, and in a state of low angular momentum ($l=0,1$). The small separation energy implies that the halo neutrons can easily be excited to continuum states. This implies that in the scattering of the halo nucleus, excitations to continuum states occur with high probability, and this should affect the optical potential of the halo nucleus, as well as its elastic scattering. It is well known that for the ${}^6,{}^7\text{Li}$ isotopes the dynamical polarization potential (the deviation of the nucleus-nucleus optical potential from its folded potential with the exchange due to the antisymmetrization between the nuclei omitted¹⁾) is necessary.^{2),3)} In these cases, simple folding models based on the nuclear single-particle densities fail to generate the optical potential that is needed to describe the elastic scattering angular distributions. The dynamical polarization potential (DPP) is expected to be very important for the halo nuclei, because the continuum states play a primary role, as only few or no bound excited states exist.^{4),20)}

The elastic differential cross section of the ${}^6\text{He}+{}^{12}\text{C}$ has been analyzed recently at 38.3 MeV/nucleon.⁶⁾ The authors of that work were unable to simultaneously account for the first deep minimum and the third high maximum using a double-folding model. They were able to account for the data only by introducing a dynamical polarization potential in a phenomenologically, and in this procedure, they had to add four free parameters, as they emphasized.

The inclusion of continuum states is carried out using a continuum-discretized

coupled-channel (CDCC) method,^{3),7),8)} in which the continuum states of the projectile are approximated by a set of discrete states, each of which couples with the relative motion between the projectile and the target.

At energies higher than 100 MeV/nucleon, the CDCC calculation becomes very difficult, because it involves a large number of partial waves. Moreover, it assumes a rigid core, which implies that the core excitation is not taken into account. By contrast, the eikonal approximation⁹⁾ is very effective at medium and high energies, and it also has the merit of simplicity.

The energy and target dependence of the breakup effect on the elastic scattering of ${}^6\text{Li}$ are studied in Ref. 7) within a CDCC framework. The continuum states of ${}^6\text{Li}$ have a simple two-body $\alpha + d$ structure. The energies studied cover the range from 5 to 30 MeV/nucleon, and the masses cover the range $A=12$ to 208. The author of that work found that the breakup effect depends little on the target and energy. Also, the breakup effect on the elastic scattering of ${}^{11}\text{Li}+{}^{12}\text{C}$ at 60 MeV/nucleon is studied in Ref. 20) in the few-body approach of the eikonal approximation.

A full eikonal calculation with a full 6-body ${}^6\text{He}$ wave function has been carried out for ${}^6\text{He}+{}^{12}\text{C}$.¹⁰⁾ With this calculation, the experimental data of Ref. 6) have been reproduced without any free parameters. Also, the relative importance of the halo neutrons and the core-nucleon excitation due to the nuclear force in the elastic scattering of ${}^6\text{He}+{}^{12}\text{C}$ as well as the energy dependence of the DPP have been studied.¹¹⁾

The present work is a completion and extension of our previous work.¹¹⁾ The purpose is to study the energy dependence of the breakup effect in more detail than in Refs. 7), 10) and 11). The energies studied here cover the range from 50 MeV/nucleon to 800 MeV/nucleon, in order to clarify the difference between the DPP of ${}^6\text{He}$ and ${}^6\text{Li}$ and to study if the sign change of the DPP at 200 MeV/nucleon found in Ref. 11) depends on the projectile/target. We now list the characteristic points and the strengths of the present approach. Firstly, ${}^6\text{He}$ and ${}^6\text{Li}$ are described with realistic (6-nucleon) wave functions which are obtained using variational Monte Carlo (VMC) calculations.¹²⁾ This makes it possible to include both core and two nucleon excitations. Secondly, the scattering amplitude is calculated with use of a Monte Carlo integration to all orders in the eikonal approximation.

In §2 we briefly summarize the basic formulae to calculate the phase shift functions. The calculation of the DPP is summarized in §3. The results are given in §4. A brief summary is given in §5.

§2. Eikonal phase

2.1. Nucleon-nucleus

The Glauber theory provides us with an excellent framework to describe high energy reactions in various fields of physics. The optical phase shift function (the elastic S -matrix) for the nucleon-nucleus is given by⁹⁾

$$e^{i\chi(\mathbf{b})} = \langle \psi_0 | \prod_{i \in P} [1 - \Gamma_{NN}(\mathbf{b} + \mathbf{s}_i)] | \psi_0 \rangle, \quad (2.1)$$

where ψ_0 is the intrinsic (translation-invariant) wave function of the projectile's ground state, \mathbf{b} is the impact parameter perpendicular to the beam (z) direction and \mathbf{s}_i is the projection onto the xy -plane of the nucleon coordinates relative to the projectile's center-of-mass. With $\Gamma_{NN}(\mathbf{b}) = 1 - e^{i\chi_{NN}(\mathbf{b})}$ the profile function Γ for the NN scattering is usually parametrized in the form

$$\Gamma_{NN}(\mathbf{b}) = 1 - e^{i\chi_{NN}(\mathbf{b})} = \frac{1 - i\alpha}{4\pi\beta} \sigma_{NN} e^{-\frac{\mathbf{b}^2}{2\beta}}, \quad (2.2)$$

where χ_{NN} is the nucleon-nucleon phase shift function, α is the ratio of the real to imaginary part of the NN scattering amplitude in the forward direction, σ_{NN} is the total NN cross section, and β is the slope parameter of the NN elastic differential cross section. The phase shift function given in Eq. (2.1) contains the effect of coupling to various inelastic channels, including the continuum states.

The phase shift $\chi_f(\mathbf{b})$, corresponding to the folded potential of the nucleon-nucleus is given by

$$\chi_f(\mathbf{b}) = \langle \psi_0 | \sum_j \chi_{NN}(\mathbf{b} + \mathbf{s}_j) | \psi_0 \rangle, \quad (2.3)$$

and, contains no coupling effect. Thus the phase shift responsible for the DPP, χ_{DPP} , is defined by

$$\chi_{\text{DPP}}(\mathbf{b}) = \chi(\mathbf{b}) - \chi_f(\mathbf{b}). \quad (2.4)$$

2.2. Nucleus-nucleus

As we introduced in Ref. 13), we consider nucleon-target (NT) scattering as an elementary reaction in the Glauber theory by assuming the target to be a scatterer and introduced a phase shift function χ_{NT} for the NT scattering. In this formalism, various effects, such as the Fermi motion, Pauli correlations, short-range dynamic correlations, etc., are automatically included to some extent in the NT phase shift determined from the NT optical potential. In the framework of this approach the nucleus-nucleus optical phase shift function (the elastic S -matrix) is defined by¹³⁾

$$e^{i\chi(\mathbf{b})} = \langle \psi_0 | \exp \left[i \sum_{i \in P} \chi_{NT}(\mathbf{b} + \mathbf{s}_i) \right] | \psi_0 \rangle. \quad (2.5)$$

The nucleon-target (NT) phase shift function χ_{NT} in Eq. (2.5) is a basic ingredient.¹³⁾ It describes the NT scattering and is related to the NT potential V_{NT} by

$$\chi_{NT}(\mathbf{b}) = -\frac{1}{\hbar v} \int_{-\infty}^{+\infty} dz V_{NT}(\mathbf{b} + z\hat{z}), \quad (2.6)$$

where $v = \hbar K/\mu$ is the asymptotic relative velocity, with μ the reduced mass of the projectile and the target and \hat{z} is a unit vector in the z -direction.

The phase shift function Eq. (2.5) contains the effect of coupling to various inelastic channels, including the continuum states. The phase shift $\chi_f(\mathbf{b})$ corresponding to the folded potential of the nucleus-nucleus is given by²⁰⁾

$$\chi_f(\mathbf{b}) = \langle \psi_0 | \sum_j \chi_{NT}(\mathbf{b} + \mathbf{s}_j) | \psi_0 \rangle, \quad (2.7)$$

and contains no coupling effect. The phase shift responsible for the DPP is the same as that given in Eq. (2.4).

§3. Dynamic polarization potential

The relationship between the phase shift and the corresponding potential is the same as in Eq. (2.6). It is straightforward to invert the phase shift function to obtain the potential:²⁰⁾

$$U_{\text{DPP}}(R) = \frac{\hbar v}{\pi} \int_0^\infty dx \frac{\chi'_{\text{DPP}}(\sqrt{R^2 + x^2})}{\sqrt{R^2 + x^2}}. \quad (3.1)$$

To understand the behavior of the dynamic polarization potential, we attempt to predict its sign in the next subsections for the cases of both the nucleon-nucleus and the nucleus-nucleus.

3.1. Nucleon-nucleus

We recall that the first term in the dynamical polarization potential Eq. (3.1) comes from the second-order phase-shift function defined by^{10),20)}

$$\chi_{\text{DPP}}(\mathbf{b}) \approx \frac{i}{2} \langle \psi_0 | \left[\sum_j \chi_{NN}(\mathbf{b} + \mathbf{s}_j) - \chi_f(\mathbf{b}) \right]^2 | \psi_0 \rangle. \quad (3.2)$$

To relate the sign of the DPP to that of the parameters of the profile function given in Eq. (2.2), let us assume that the neutron-proton and proton-proton have the same profile functions. Then, recalling the relation between the profile function and the phase shift given by Eq. (2.2) and with the Taylor expansion, we have

$$\chi_{NN} = -i \ln(1 - \Gamma_{NN}) \approx i\Gamma_{NN} + \dots. \quad (3.3)$$

From Eqs. (3.3) and (3.2), it is seen that the leading term of the phase shift χ_{DPP} is proportional to $i(i\Gamma)^2 = i[-(1 - i\alpha)^2]$. Because the sign of the potential is opposite to the sign of the phase shift function Eq. (2.6), the sign of the real part of the leading term of the dynamical polarization potential Eq. (3.1) is the same as that of α , and the sign of the imaginary part agrees with that of $(1 - \alpha^2)$. If we assume that the NN potential has the form $V_{NN}(R) \sim (v_0 + iw_0)f(R)$, it is straightforward to show that the first term of the value of α is given by $\frac{v_0}{w_0}$.

3.2. Nucleus-nucleus

As in the nucleon-nucleus case, in the nucleus-nucleus case also the first term in the DPP Eq. (3.1), comes from the second-order phase shift function of the nucleus-nucleus. It is given by²⁰⁾

$$\chi_{\text{DPP}}(\mathbf{b}) \approx \frac{i}{2} \langle \psi_0 | \left[\sum_j \chi_{NT}(\mathbf{b} + \mathbf{s}_j) - \chi_f(\mathbf{b}) \right]^2 | \psi_0 \rangle. \quad (3.4)$$

The sign of the DPP can be predicted under certain conditions. Assuming that the V_{NT} has the form $V_{NT}(R) \sim (V_0 + iW_0)f(R)$, it is seen that χ_{DPP} is proportional

to $(i/2)(V_0 + iW_0)^2$. If the main contribution to the DPP comes from the first term, its sign is the same as that of $-i(V_0 + iW_0)^2$, and therefore the real and imaginary parts of the dynamic polarization potential have the same signs as $\frac{V_0}{W_0}$ and $1 - (\frac{V_0}{W_0})^2$, respectively. These relations are given in Refs. 3), 7) and 20).

From the above considerations, we find that the sign of the first term of the DPP in both the nucleon-nucleus and nucleus-nucleus cases is related to the ratio of the real to the imaginary parts of the underlying potential. We do not use the approximation given by Eq. (3.2) or Eq. (3.4), but, instead, we calculate the phase shift functions accurately in this paper.

§4. Results

4.1. Input data

The matrix elements given in Eqs. (2.1) and (2.5) contain multi-dimensional integrations, which obviously are not easy to perform in general. Recently, it has been demonstrated¹⁴⁾ that the phase shift function can be evaluated using Monte Carlo method without approximation. The effectiveness of that method has been illustrated by several examples, including ${}^4,6\text{He}+{}^{12}\text{C}$, and we use it in this study as well.

The wave function used for ${}^4,6\text{He}$ and ${}^6\text{Li}$ is the variational Monte Carlo (VMC) wave function.¹²⁾ The ${}^6\text{He}$ (${}^4\text{He}$) root mean square (r.m.s.) radii with the VMC wave function are 2.56 (1.46), 1.96 (1.46) and 2.81 (1.46) fm for the nucleon, proton and neutron, respectively. Those for ${}^6\text{Li}$ are 2.47, 2.47 and 2.47 fm.

For V_{NT} , we use the central part of the p -nucleus global optical potential,¹⁵⁾ ignoring the difference between p -nucleus and n -nucleus interactions. This potential is determined by the Dirac phenomenology and gives a good fit to $p+{}^{12}\text{C}$ elastic scattering data. The incident energy considered in the present study covers the energy range 50–800 MeV/nucleon. The real part of V_{NT} changes sign: It is attractive below 300 MeV, with its depth decreasing as the energy increases, and becomes repulsive in its interior region above 300 MeV. By contrast, the imaginary part is always absorptive (negative), with its depth increasing as the energy increases. Reflecting the fact that the pion production threshold for a nucleon incident on a nucleus is around 250 MeV, the depth of the imaginary potential becomes very large above that energy. It is noted that this energy dependence is common for $p-{}^{12}\text{C}$, $p-{}^{40}\text{Ca}$ and $p-{}^{208}\text{Pb}$ optical potentials,¹⁵⁾ except at 200 MeV.

To study the difference between the DPP of ${}^6\text{He}$ and ${}^6\text{Li}$, we start from the nucleon-nucleon interaction, because both np and pp parameters are known in this case.¹⁶⁾

4.2. Breakup effect on the elastic S -matrix

In order to see how the breakup effect on the elastic scattering changes with energy, we plot the S -matrix elements in the complex S plane for ${}^6\text{He}+{}^{12}\text{C}$ at energies from 50 to 800 MeV/nucleon, as a prototype calculation. This calculation was done for ${}^4,6\text{He}+p$, ${}^{12}\text{C}$, ${}^{40}\text{Ca}$ and ${}^6\text{Li}+p$. In Fig. 1, the solid curves represent the eikonal

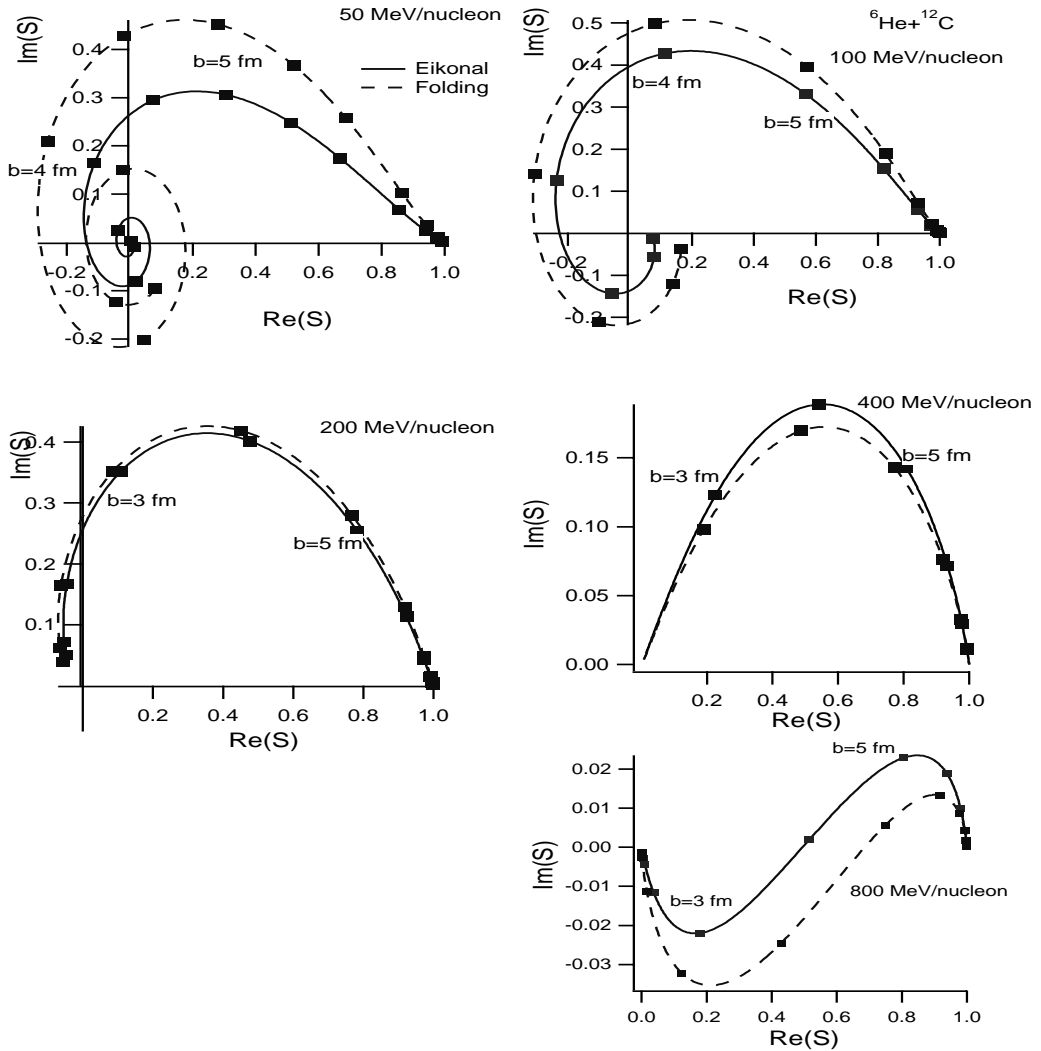


Fig. 1. The elastic S -matrix elements for ${}^6\text{He}+{}^{12}\text{C}$ at energies from 50 to 800 MeV/nucleon. The solid curve represent the eikonal calculation, while the dashed curve represent the folding calculation.

calculation, while the dashed curves represent the folding calculation. It is interesting that the inclusion of the breakup reduces the strength of the S -matrices below 200 MeV/nucleon and at 800 MeV/nucleon, while it increases them at 400 MeV/nucleon. This implies that the breakup effect is of a repulsive and an absorptive nature below 200 MeV/nucleon, almost zero at 200 MeV/nucleon, repulsive and anti-absorptive at 400 MeV/nucleon, and attractive and anti-absorptive at 800 MeV/nucleon. The minimum value of the breakup effect at 200 MeV/nucleon can be understood from the fact that the transparency of the $p-{}^{12}\text{C}$ interaction reaches its maximum near that energy.¹⁷⁾ We stress here that this behavior is the same for all the systems that we have studied.

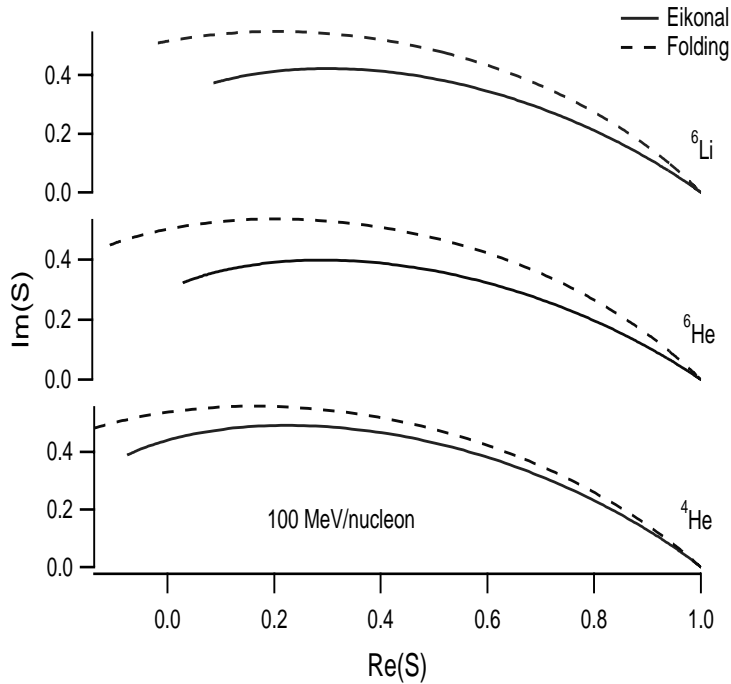


Fig. 2. The same as Fig. 1, but for ${}^4,6\text{He}$ and ${}^6\text{Li}$ incident on a proton target at 100 MeV/nucleon.

Figure 2 is the same as Fig. 1, but for the cases ${}^4,6\text{He}$ and ${}^6\text{Li}$ incident on a proton target at 100 MeV/nucleon. The solid curves represent the eikonal calculation, while the dashed curves represent the folding calculation. Two points are noted here. One is that the breakup effect in ${}^4\text{He}$ is not negligible. The second point is that the breakup effect in ${}^6\text{He}$ is slightly stronger than that in ${}^6\text{Li}$. This will be seen more clearly in the next section, where we discuss the DPP of ${}^6\text{He}$ and ${}^6\text{Li}$.

4.3. The DPP

The breakup effect in the potential form is shown in Fig. 3. The real and imaginary parts of the DPP for ${}^6\text{He}+p$, ${}^{12}\text{C}$ and ${}^{40}\text{Ca}$ are represented by the dotted, dashed and solid curves respectively, at 100, 200 and 400 MeV/nucleon. The imaginary part of the DPP is negative below 200 MeV/nucleon, but turns out to be positive above 200 MeV/nucleon. This sign change is related to the transparency of the p -nucleus, which reaches its maximum around that energy,¹⁷⁾ as we discussed in the previous section. We can understand this sign change, as discussed in §3, from the value of $1 - (\frac{V_0}{W_0})^2$ ($1 - \alpha^2$ in the case of ${}^6\text{He}+p$). It is negative below 200 MeV/nucleon, while it is positive above 200 MeV/nucleon. The real part of the DPP for ${}^6\text{He}+{}^{12}\text{C}$ and ${}^{40}\text{Ca}$ also changes sign from positive to negative around 400 MeV/nucleon. This sign change can also be understood from the value $\frac{V_0}{W_0}$ of $p-{}^{12}\text{C}$ and $p-{}^{40}\text{Ca}$ optical potentials. It is positive below 300 MeV/nucleon and negative above that energy. For the real part of ${}^6\text{He}+p$, it changes sign at 650 MeV/nucleon, because the value of α becomes negative at that energy. Next, we examine the dependence of the DPP

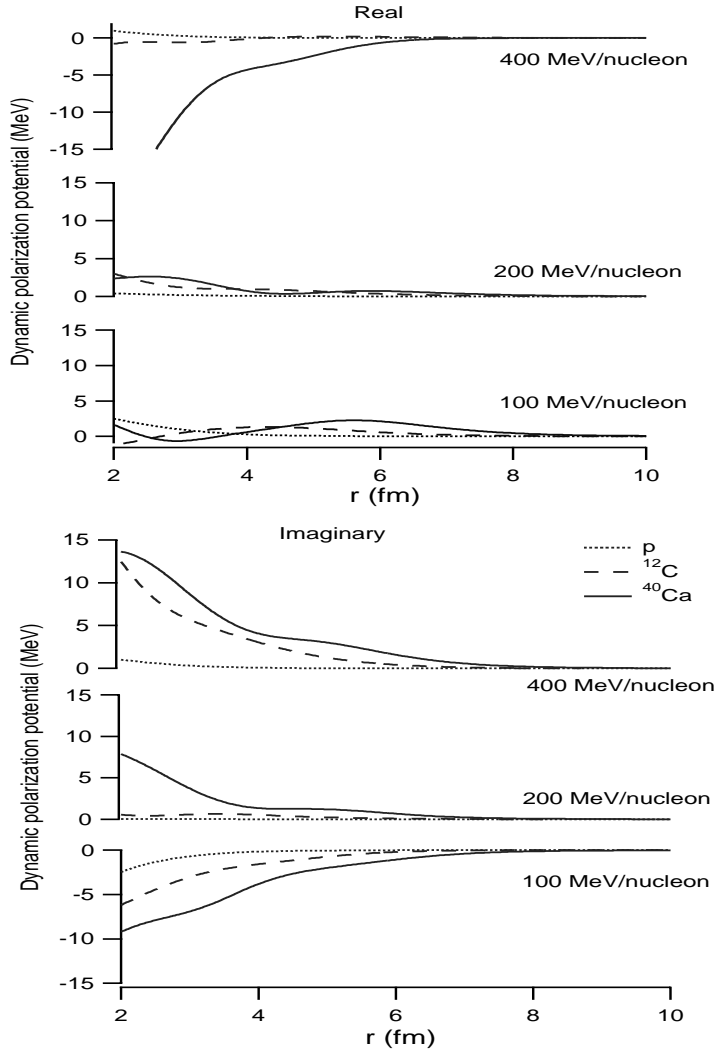


Fig. 3. The real and imaginary parts of the DPP for ${}^6\text{He}+p$ (dotted curve), ${}^{12}\text{C}$ (dashed curve) and ${}^{40}\text{Ca}$ (solid curve) at 100, 200 and 400 MeV/nucleon.

on the target nucleus. We calculated the potential for ${}^{12}\text{C}$ and ${}^{40}\text{Ca}$ targets at an incident energy of 100 MeV/nucleon. Figure 4 shows the ratio of the DPP to the folding potential. The dashed and solid curves represent the calculations for ${}^{12}\text{C}$ and ${}^{40}\text{Ca}$ targets, respectively. The ratios of the potentials are similar for the two targets and have approximately the same value in the peripheral region. This behavior is the same as that found in Ref. 7).

Figure 5 shows the real and imaginary parts for the DPP of ${}^6\text{He}+p$ (solid curves) and ${}^6\text{Li}+p$ (dashed curves) compared to those of ${}^4\text{He}+p$ (dotted curves) at 100 MeV/nucleon. The difference between the DPP of ${}^6\text{He}$ and that of ${}^4\text{He}$ is due to the effect of the halo-neutrons breakup. The real (imaginary) parts of the volume integral $J = \int dr V_{\text{DPP}}(r)/A$ (in units of MeV fm³) are 19 (−26), 66 (−58) and 53

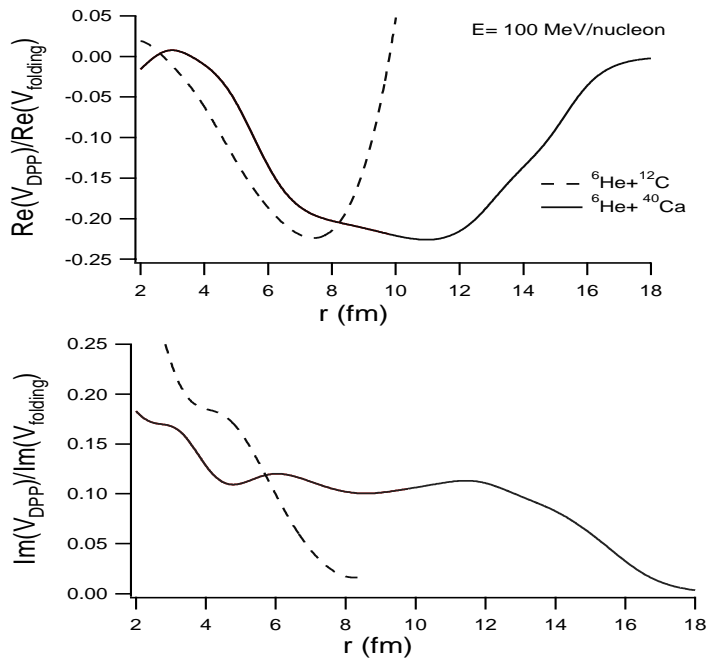


Fig. 4. The ratio of the DPP to the folding potential for ${}^6\text{He}+{}^{12}\text{C}$ (solid curve), ${}^{40}\text{Ca}$ (dashed curve) at 100 MeV/nucleon.

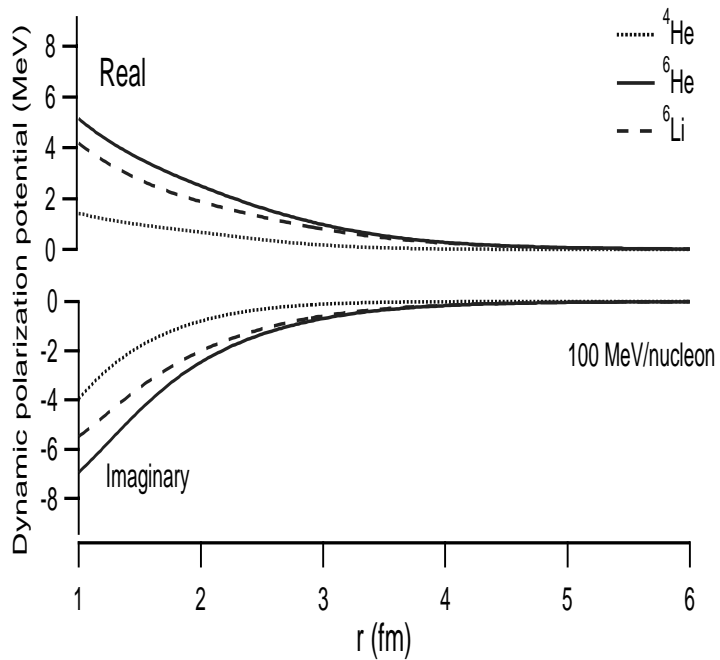


Fig. 5. The same as Fig. 3, but for ${}^4,6\text{He}$ and ${}^6\text{Li}$, at 100 MeV/nucleon.

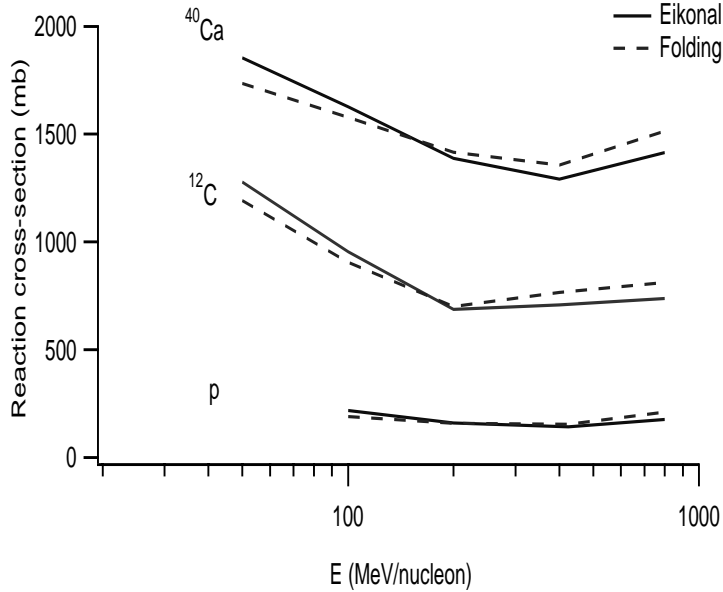


Fig. 6. The reaction cross section as a function of the incident energy per nucleon for ${}^6\text{He}+p$, ${}^{12}\text{C}$ and ${}^{40}\text{Ca}$. The solid curves are the eikonal calculation, while the dashed curves represent the folding calculation.

(-48) for ${}^4\text{He}$, ${}^6\text{He}$, and ${}^6\text{Li}$ respectively. One noteworthy point here is that the DPP of ${}^6\text{He}+p$ is stronger than that of ${}^4\text{He}+p$ and has a longer range. This feature is related to the halo structure of ${}^6\text{He}$. Also, the effect of the halo-neutrons breakup is stronger than that of the core (${}^4\text{He}$). The second point is that the breakup effect for ${}^6\text{He}$ is stronger than that for ${}^6\text{Li}$. To clarify the origin of this relation, we repeated the calculation for ${}^6\text{He}$, assuming it contains three protons. Here, the neutron-target (proton) interaction for one of the neutrons in ${}^6\text{He}$ is just replaced with the proton-target (proton) interaction in Eqs. (2.1) and (2.2) to simulate the ${}^6\text{Li}$ case, but using the ${}^6\text{He}$ wave function. The result of this calculation coincides with that for ${}^6\text{Li}$. Therefore the difference between the DPP of ${}^6\text{He}$ and that of ${}^6\text{Li}$ at 100 MeV/nucleon is mainly due to their charge difference.

We now discuss the breakup effect on the reaction cross sections. We decompose the reaction cross section into two terms, as

$$\begin{aligned}\sigma_R &= \int d\mathbf{b} (1 - |e^{i\chi(\mathbf{b})}|^2) \\ &= \int d\mathbf{b} (1 - |e^{i\chi_f(\mathbf{b})}|^2) + \int d\mathbf{b} |e^{i\chi_f(\mathbf{b})}|^2 (1 - |e^{i\chi_{\text{DPP}}(\mathbf{b})}|^2),\end{aligned}\quad (4.1)$$

where $|e^{i\chi_f(\mathbf{b})}|^2$ is the survival probability of the incident flux subjected to the absorption of the folding potential. The reaction cross section calculated from the first term is called the optical limit value. The above decomposition is carried out to emphasize the role of the DPP on the reaction cross section. Figure 6 shows the reaction cross sections of ${}^6\text{He}+p$, ${}^{12}\text{C}$ and ${}^{40}\text{Ca}$ at energies from 50 to 800 MeV/nucleon.

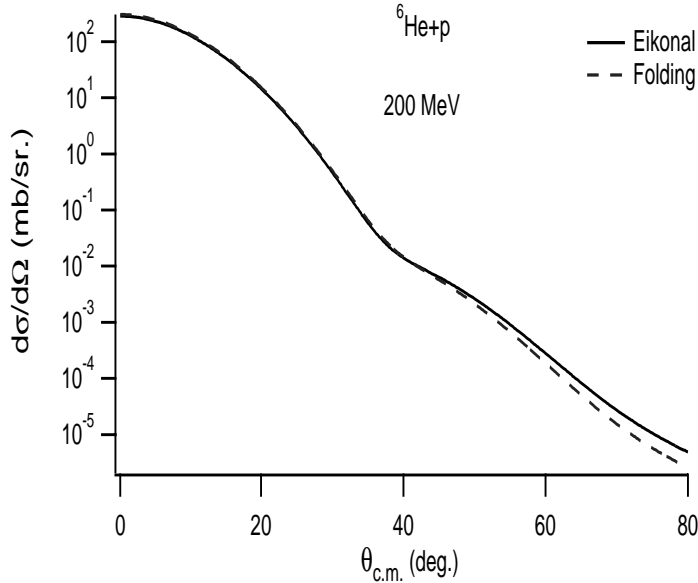


Fig. 7. The elastic differential cross section for ${}^6\text{He}+p$ at 200 MeV/nucleon. The solid curve represents the eikonal calculation, while the dashed curve represents the folding calculation.

The solid curves represent the eikonal calculation, while dashed curves represent the folding calculation, the first term in Eq. (4.1). As we see, the DPP gives a positive contribution to σ_R at energies lower than 200 MeV/nucleon, while it gives a negative contribution at energies higher than 200 MeV/nucleon. That is, the optical limit approximation underestimates the reaction cross section below $E=200$ MeV/nucleon but overestimates it above 200 MeV/nucleon. The overestimation by the optical-limit approximation has been pointed out by several authors,^{18),19)} and the underestimation is demonstrated in Ref. 20). This behavior is related to the sign of $1 - |e^{i\chi_{\text{DPP}}(\mathbf{b})}|^2$, in other words to whether the quantity $|e^{i\chi_{\text{DPP}}(\mathbf{b})}|^2$ is greater than or less than 1. This depends on the sign of the imaginary part of the DPP. As discussed above, the sign of the imaginary part of the DPP is negative below 200 MeV/nucleon, and therefore $1 - |e^{i\chi_{\text{DPP}}(\mathbf{b})}|^2$ becomes positive, while at energies higher than 200 MeV/nucleon, the sign of the imaginary part of the DPP is positive, and therefore $1 - |e^{i\chi_{\text{DPP}}(\mathbf{b})}|^2$ becomes negative. Also, we see that the eikonal calculation and the folding calculation coincide at 200 MeV/nucleon. This is because the DPP becomes minimal at this energy.

The breakup effect becomes minimal at 200 MeV/nucleon. For example the reaction cross sections obtained from the eikonal and folding calculations for ${}^6\text{He}+{}^{12}\text{C}$ at 200 (800) MeV/nucleon are 686 (737) and 700 (811) mb, respectively. The difference is only 2% at 200 MeV/nucleon, while it is 10% at 800 MeV/nucleon. Also, the differential elastic cross sections obtained using the eikonal and folding calculations for the same system coincide up to 10 degrees at 200 MeV/nucleon. For ${}^6\text{He}+p$ and at 200 MeV/nucleon, the reaction cross sections obtained with the eikonal and folding calculations are 173 and 174 mb, respectively. The elastic differential cross

section for ${}^6\text{He}+p$ calculated at 200 MeV/nucleon is shown in Fig. 7. The solid curve represents the eikonal calculation, while the dashed curve represents the folding calculation. It is clearly seen that the two calculations coincide for this system at that energy. Therefore, the calculation for a proton target at 200 MeV/nucleon can be considered model independent.

§5. Summary

The eikonal approximation is valid for medium and high energies. We have used its utility to calculate the elastic optical phase shift function (S -matrix) for ${}^4,6\text{He}+p$, ${}^{12}\text{C}$, ${}^{40}\text{Ca}$ and ${}^6\text{Li}+p$ at medium energies, 50–800 MeV/nucleon. Both the halo-neutrons and the core-nucleon excitations were taken into account by using realistic wave functions generated by variational Monte Carlo calculations. The p -nucleus optical potential were used as a basic input for ${}^6\text{He}+{}^6\text{C}$ and ${}^{40}\text{Ca}$. Also, the np and pp parameters were used for ${}^4,6\text{He}+p$ and ${}^6\text{Li}+p$ to distinguished between ${}^6\text{He}$ and ${}^6\text{Li}$. The polarization potentials have been calculated. We report that the breakup effect is a minimum at 200 MeV/nucleon. The breakup effect gives a positive contribution to the reaction cross section at energies lower than 200 MeV/nucleon, while it gives a negative contribution at energies higher than 200 MeV/nucleon. We also find that the imaginary part of the DPP changes sign from negative to positive around 200 MeV/nucleon. The real part also changes sign from positive to negative around 400 MeV/nucleon for ${}^6\text{He}$ +nucleus (in which case the p -nucleus potential is used as a basic input). For ${}^4,6\text{He}+p$ and ${}^6\text{Li}+p$ (in which case the NN -parameter is used as a basic input), the sign change occurs at 650 MeV. The sign change depends neither on the projectile nor on the target; it depends only on the ratio of the real to the imaginary parts of the underlying nucleon-nucleon (or nucleon-target) potential. The effect of the halo-neutron excitations is larger than that of the core (${}^4\text{He}$) for ${}^6\text{He}$. The breakup effect for ${}^6\text{He}$ is stronger than that for ${}^6\text{Li}$. This is mainly due to the charge difference between ${}^6\text{Li}$ and ${}^6\text{He}$.

Acknowledgements

The author is very much indebted to Professor Y. Suzuki for useful discussions. This work is supported by a JSPS Postdoctoral Fellowship for Foreign Researchers (No. P03023).

References

- 1) H. Feshbach, *Ann. of Phys.* **19** (1962), 287.
- 2) G. R. Satchler and W. G. Love, *Phys. Rep.* **55** (1979), 184.
- 3) Y. Sakuragi, M. Yahiro and M. Kamimura, *Prog. Theor. Phys. Suppl. No. 89* (1986), 136.
- 4) Y. Suzuki, R. G. Lovas, K. Yabana and K. Varga, *Structure and reactions of light exotic nuclei* (Taylor & Francis, London, 2003).
- 5) K. Yabana, Y. Ogawa and Y. Suzuki, *Phys. Rev. C* **45** (1992), 2909.
- 6) V. Lapoux et al., *Phys. Rev. C* **66** (2002), 034608.
- 7) Y. Sakuragi, *Phys. Rev. C* **35** (1987), 2161.
- 8) T. Matsumoto, E. Hiyama, M. Yahiro, K. Ogata, Y. Iseri and M. Kamimura, *Nucl. Phys. A* **738** (2004), 471c.

- 9) R. J. Glauber, in *Lectures on Theoretical Physics*, ed. W. E. Brittin and L. C. Dunham (Interscience, New York, 1959), Vol. 1, p. 315.
- 10) B. Abu-Ibrahim and Y. Suzuki, Nucl. Phys. A **728** (2003), 118; *ibid.* **732** (2004), 218.
- 11) B. Abu-Ibrahim and Y. Suzuki, Phys. Rev. C **70** (2004), 011603(R).
- 12) B. S. Pudliner, V. R. Pandharipande, J. Carlson, S. C. Pieper and R. B. Wiringa, Phys. Rev. C **56** (1997), 1720.
- 13) B. Abu-Ibrahim and Y. Suzuki, Phys. Rev. C **61** (2000), 051601(R); Phys. Rev. C **62** (2000), 034608.
- 14) K. Varga, S. C. Pieper, Y. Suzuki and R. B. Wiringa, Phys. Rev. C **66** (2002), 034611.
- 15) E. D. Cooper, S. Hama, B. C. Clark and R. L. Mercer, Phys. Rev. C **47** (1993), 297.
- 16) L. Ray, Phys. Rev. C **20** (1979), 1857.
- 17) R. M. DeVries and J. C. Peng, Phys. Rev. Lett. **43** (1979), 1373.
- 18) Y. Ogawa, K. Yabana and Y. Suzuki, Nucl. Phys. A **543** (1992), 722.
- 19) J. S. Al-Khalili and J. A. Tostevin, Phys. Rev. Lett. **76** (1996), 3903.
- 20) K. Yabana, Y. Ogawa and Y. Suzuki, Nucl. Phys. A **539** (1992), 295.